

DETECTION AND MEASUREMENT OF POORLY SAMPLED POINT SOURCES IMAGED WITH 2-D ARRAYS

STEVE B. HOWELL

Planetary Science Institute, Astrophysics Group, 620 North 6th Avenue, Tucson, Arizona 85705 and Department of Physics and
Astronomy, University of Wyoming, P.O. Box 3905, University Station, Laramie, Wyoming 82071
Electronic mail: showell@kaya.uwyo.edu

BRUCE KOEHN AND EDWARD BOWELL

Lowell Observatory, 1400 Mars Hill Road, Flagstaff, Arizona 86001
Electronic mail: koehn@lowell.edu, elgb@lowell.edu

MARK HOFFMAN

Department of Astronomy, Yale University, New Haven, Connecticut 06520
Electronic mail: mark.hoffman@yale.edu

Received 1995 Dec. 1; revised 1996 April 3

ABSTRACT

Imaging systems in which the pixels are large compared to the point spread function produce undersampled data for which traditional 2-D Gaussian PSF fitting will not work well. Such systems include wide-field imaging applications (CCD mosaics) and space-based telescopes. The current astronomical literature provides few recipes to use when dealing with undersampled data. We present a method of providing optimum signal-to-noise data matching for poorly sampled point sources which makes use of profile fitting but only within small, variable-size pixel masks. A wide-field imaging Schmidt telescope project, Lowell Observatory Near-Earth Object Search (LONEOS), is discussed as an example. Our pixel mask technique is applied to model images from the LONEOS camera, and we show that we can determine point-source centroids and brightnesses with good precision, even for faint objects. © 1996 American Astronomical Society.

1. INTRODUCTION

Two-dimensional arrays, in particular charge-coupled devices (CCDs), are the mainstay optical observational tool today. The use of these rectangular silicon marvels have become commonplace in both professional and non-professional astronomy, and has resulted in numerous new discoveries and observational techniques. However, CCDs are not perfect, and the more we expect from them, the more knowledgeable we need to become about them.

Observers of point sources are mainly interested in astrometry and photometry, seeking precise magnitudes and positions even in the extreme digital environments of faint sources and large projected area per CCD pixel. These are the realms of working with very low signal-to-noise (S/N) data that are marginally or poorly sampled. Digital images from space (e.g., *Hubble Space Telescope*, Holtzman 1990 and Holtzman *et al.* 1995; and the Galileo Spacecraft, e.g., Howell & Merline 1991), have caused some problems, such as undersampling and cosmic ray identification, to become forefront in users' minds. Renewed interest in large-field Schmidt telescopes with CCD mosaics for large-area coverage or in digital sky surveys have also caused us to rethink our standard data analysis procedures. These are exciting new areas of application for CCDs, but to date, the scientific literature is sparse on detailed studies.

Work on marginally sampled or undersampled data has

appeared in a few articles (e.g., Buonanno & Iannicola 1989, Holtzman 1990, Howell 1995) and work with very low S/N point-source data has also been mentioned in the literature (Stetson 1987, Howell 1989). We present here a detailed study of a method that can be successfully used to detect and measure, with good precision, poorly sampled point sources, even those of low S/N, imaged on 2-D arrays.

The driving motivation for this work is our involvement with the Lowell Observatory Near-Earth Object Search (LONEOS). This project, should be able to provide us with monthly digital imaging of the entire dark sky. The system will use a CCD mosaic and a Schmidt telescope, and will obtain information on objects over the magnitude range of 14th to 19th or fainter. At 2.8 arcsec per pixel, we will be swimming in a digital sea of poorly sampled, and (at the faint end) low-S/N data. In Sec. 2, we provide an introduction to some needed terminology. In Sec. 3, we briefly describe the LONEOS project, in Sec. 4 discuss the detection and measurement procedures, and in Sec. 5 present our results.

2. SIGNAL-TO-NOISE, PIXEL SAMPLING, AND PSF FITTING

2.1 Signal-to-Noise

Signal-to-noise (S/N) is a term frequently encountered when one reads about digital astronomical measurements. In principle, S/N is easy to understand for a 2-D point-source

TABLE 1. Terms in Eq. (1).^a

Parameter	Description	Units
N_{\star}	Total source photons	electrons
n_{pix}	Total number of pixels in source aperture	...
n_B	Total number of pixels in background (sky) aperture	...
N_S	Total background (sky) counts/pixel	electrons
N_D	Total dark counts/pixel	electrons
N_R	Read noise/pixel	electrons
G	Gain of detector	electrons/ADU ^b
σ_f	1 σ of fractional count lost to digitization/pixel (~ 0.289)	ADU ^b

^aSee Merline & Howell (1995) for a complete description.

^bADU=Analog-to-digital unit, sometimes called DN (Data Number).

measurement. It is the ratio of the signal (source photons) to the noise (noise photons or other pseudo photons) present in an observation. However, in practice, quoted S/N ratios can be misleading unless one is certain *how* they were calculated.

Knowing the precise meaning of the S/N is very important for discussions of poorly sampled data, as each point source is contained within only a few pixels. The correct expression for calculation of a S/N for a given CCD observation involves some quantities that are instrument dependent and quantities that are arbitrarily chosen by the user. With no knowledge of what values were chosen, the S/N is meaningless. The equational representation for the S/N for a single CCD observation of a point source is given by Merline & Howell (1995):

$$\frac{S}{N} = \frac{N_{\star}}{\sqrt{N_{\star} + n_{\text{pix}} \left(1 + \frac{n_{\text{pix}}}{n_B} \right) (N_S + N_D + N_R^2 + G^2 \sigma_f^2)}}, \quad (1)$$

where the terms are defined in Table 1. While this equation can be applied to a given CCD observation, it may not always be meaningful, especially when used indiscriminately (Howell 1993).

To give the reader an appreciation for the kind of data we are dealing with in this paper, Fig. 1 is included to illustrate some aspects of a 2-D image. The models have been calculated using the method described in Merline & Howell (1995), and from our work here described in Sec. 3. The figure shows two cases of interest. A bright and faint source imaged with a typical well-sampled CCD system, and the same sources as they appear when poorly sampled by LO-NEOS models. Notice in Fig. 1 that, as the S/N and the sampling get worse, the point spread functions (PSFs) appear much less Gaussian in profile, and hence become much less amenable to traditional 2-D profile fitting (e.g., Stetson 1987), aperture photometry (e.g., Adams *et al.* 1980), or optimal filtering techniques (e.g., Goad 1986, Abbott 1993). For a given telescope, instrument, and CCD combination, the user can always pick n_{pix} and n_B to yield an optimum S/N (Howell 1989). However, to perform this work effectively in the case of low-S/N or poorly sampled data, new techniques, involving non-traditional methods of analysis are needed.

2.2 Pixel Sampling and PSF Fitting

Undersampled or marginally sampled data are also terms that must be defined. Buonanno & Iannicola (1989) and Howell (1995) discuss what is called the sampling parameter r , defined as

$$r = \frac{\text{FWHM}}{p}. \quad (2)$$

FWHM is the full width at half maximum of the stellar PSF and p is the pixel size, both in the same units (e.g., arcseconds). For $r \leq 1.5$, the data are considered undersampled. One may expect increasing errors with decreasing r in both photometry and astrometry if standard analysis techniques (e.g., Adams *et al.* 1980) are used because most data reduction packages were designed for and only provide good results for well-sampled point-source data. The normal mode of 2-D Gaussian (or smooth spline)¹ profile fitting begins to fail for poorly sampled or low-S/N data. In the specialized regime of small r , sophisticated techniques are needed to treat each pixel individually.

For $r \sim 1.5$, data are considered marginally sampled, in which case the choice of analysis techniques is highly dependent on the S/N of the data themselves. In fact, as we discuss below, hybrid analysis techniques, based on total source counts, are well suited to such tasks. These techniques provide optimum data extraction using measurement parameters which are changeable on the fly depending on the S/N present in any given point source.

We see clearly from Fig. 1 that typical 2-D fitting techniques will not represent the actual data once we move towards the low-S/N, undersampled regime. Almost all of these techniques are exclusively designed for good- to high-S/N, well-sampled data; i.e., data that, to a good approximation, represent a 2-D azimuthally symmetric continuous function, such as a Gaussian. Such fits overestimate the pro-

¹Note that many common software packages present plots of PSFs and other quantities as spline fits to the data. These "smooth" plots are often misleading to the user when applied to sources that are marginally sampled or of low S/N. They tend to give the appearance that the data are always well sampled and Gaussian in nature. Such plots also display the local background (sky) to make it appear smooth and nearly constant in value. Plots presented as pixel histograms, as in Fig. 1, show the real aspect of the data and allow the user a deeper understanding of what the software must be applied to.

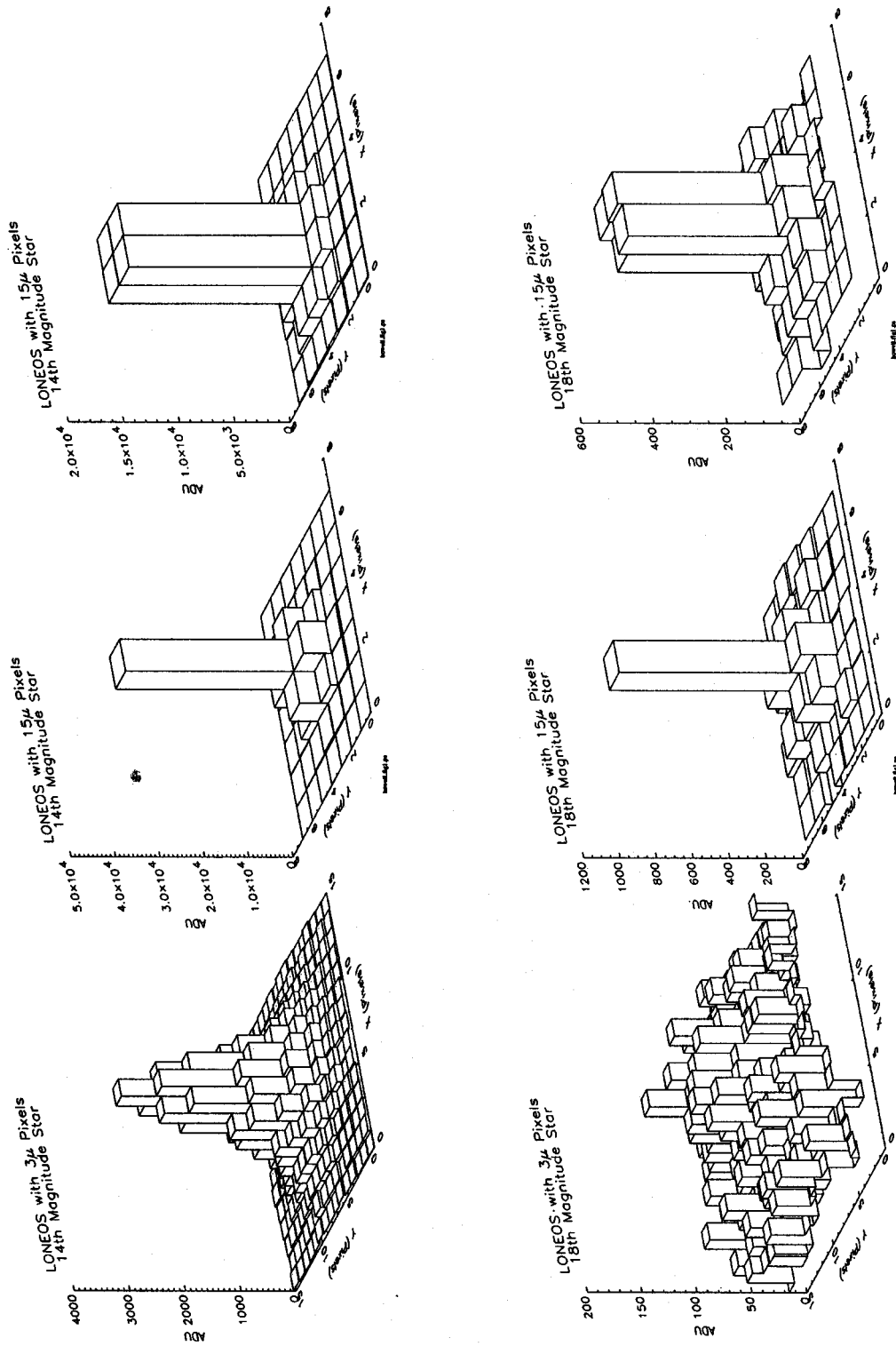


FIG. 1. Six PSFs compared. The left two panels show bright and faint stars imaged with the LONEOS camera if it had 3μ pixels. The middle panels show the same two stars as they may appear in actual LONEOS data; i.e., poorly sampled. Note, however, how the fainter star is helped by the large pixel size. The right two panels again show the same two LONEOS stars but they are now not centered within a pixel but near a corner. The high-S/N, well sampled star (top left) looks like and can be well approximated by a Gaussian PSF. Even a well-sampled, lower S/N image can be analyzed using the same technique with some success. The poorly sampled images (4 panels on the right hand side) cannot be well approximated by a Gaussian function.

file near the center, fail to provide a correct background reference in the wings, and cause background counts to be included as source signal. Noting these shortcomings of the standard methods, we have developed a hybrid approach in which we use the true, non-Gaussian PSF (obtained from the data themselves), sample this PSF in a highly pixelized manner appropriate to the data, and “profile fit” the low-S/N, poorly sampled point sources on a limited pixel-by-pixel basis using an optimum rectangular mask. This type of analysis *must* be undertaken to obtain precise results from poorly sampled data.

3. EXAMPLE SYSTEM — LONEOS

The LONEOS project is designed to provide areal sky scanning in order to locate large asteroids and comets in near-Earth orbits (Near-Earth Objects = NEOs). “Large” objects will typically be asteroids greater than 0.5 km in diameter and comets that become brighter than about $V=19.5$ mag (Bowell & Muinonen 1994; Schoemaker 1995). The digital sky scans will also be used for variable star and galaxy monitoring and discovery, and as a testbed to search for photometric evidence of transits by extra-solar planets. These additional “piggy-back” science projects will not be discussed further here. The LONEOS system will be able to survey up to ~ 2600 square degrees of sky per night, with a single scan region being 3.2 by 30 degrees in size. The minimum effective integration time can be as short as 34 sec, though for modeling reported here we suppose an integration time of 68 sec.

To achieve the required areal coverage, the LONEOS system will make use of a Schmidt telescope having a 60 cm primary aperture and 58 cm corrector plate. The focal length of 111 cm provides an $f/1.91$ focal ratio and the effective aperture is 44 cm. A field flattener placed just ahead of the CCD detectors will keep the entire image focused on the CCD plane and reduce the optical aberrations at the edge of the field of view. The LONEOS telescope is located on Anderson Mesa, southeast of Flagstaff, Arizona. Further details of the CCD and camera design can be found in Diercks *et al.* (1995).

Each CCD pixel has a 350,000-electron full-well capacity, though for simplicity of automated operation the LONEOS camera will be operated in Multi-Pinned Phase (MPP) mode to reduce the dark current when using only thermoelectric cooling. This reduces each pixel full well to $\sim 100,000$ electrons. A 14-bit A/D converter will be used with a gain of $6e^-/\text{DN}$. The expected quantum efficiency of the startup CCDs peaks at about 40% near $0.65 \mu\text{m}$ and falls almost linearly to zero at 0.38 and $1.0 \mu\text{m}$. The LONEOS camera will operate unfiltered, giving an approximate effective bandpass for the initial CCDs of $\lambda_c \sim 6500 \pm 2000 \text{ \AA}$. The CCD should have a read noise of 32 electrons, a dark current of 9 electrons/sec, and a sky contribution of 116 electrons/sec. We find from our models that a 17th magnitude, A star will have 14610 DN for the 68-sec effective exposure. The pixel size of $15 \mu\text{m}$ and image scale of 186 arcsec/mm provide a field of view of 3.17 deg (width) at 2.8 arcsec/pixel. Using typical Anderson Mesa seeing and

the optical design ray traces, the sampling parameter for LONEOS will be $r = 2/2.8 \sim 0.7$. Most NEO detections and point source images will be poorly sampled by the LONEOS system, with a typical PSF covering an area of only 4 to 6 pixels.

All objects on the scans will be processed to provide astrometric (x,y) and photometric (I) information. The software must perform these tasks as fast as possible as we can not afford to fall behind in data reduction. The raw data will be saved for further detailed analysis if needed, and for archival purposes, while most remaining work will deal only with the (x,y,I) lists. The imaged sources will be analyzed and will have their (x,y,I) information stored in a database. Currently, we are planning on setting the initial detection limit at $\sim 3\sigma$ above the background, which is near a magnitude limit of $V \sim 20$ mag.

The astrometric and photometric work on all objects of interest makes use of our technique for analyzing poorly sampled data, discussed in Sec. 4. The technique, as implemented for LONEOS, consists of two parts: generating template point spread functions, and finding the optimum match between this template and a potential point source detection. In this paper, template PSFs have been model generated, but during actual LONEOS operation they will be formed from large numbers of high-S/N point sources imaged on the LONEOS scans.

4. MODEL DATA, DETECTION, AND MEASUREMENT TECHNIQUES

Before testing our algorithms, we needed to generate, as realistically as possible, model 2-D data approximating those obtained with LONEOS. The calculations involved four major areas: calculation and calibration of the total light entering the telescope and registering on the detector, calculation of the noise from the sky and other sources, calculation of dispersive effects, and modeling the CCD detectors in a realistic fashion. We used the absolutely known flux of Vega (Tüg *et al.* 1977) as our starting point, and then calculated the total irradiance at the CCD. Redder spectra of asteroids and bluer spectra of hot stars were allowed for in the calculations as needed. We accounted for reflection and absorption losses in the telescope optics, the areas of the corrector plate and mirror, and the light blocked by the camera dewar and spider. The DQE curve of the CCDs was included in the integration over all appropriate wavelengths. Merline & Howell (1995) give details of such a calculation leading to the production of realistic models of point-source images.

The sky background was calculated using the night-sky spectrum published by Massey *et al.* (1990). Effects such as the expected read noise and dark current (but not cosmic-ray strikes) were included (see Merline & Howell 1995) to provide a reasonably accurate picture of noise sources. Other dispersive effects considered were atmospheric extinction, charge blurring caused by the near-quantized motion of the pixel charge as it is row-shifted through the CCD (operating in scan mode), misalignment between the CCD columns and the declination axis, atmospheric refraction, and dispersion in the telescope optics.

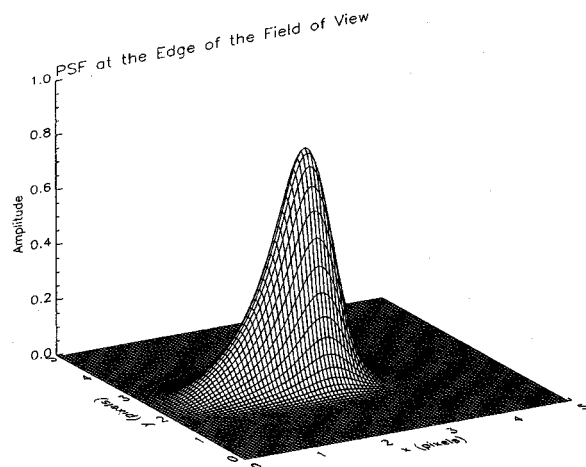


FIG. 2. A noiseless asymmetric PSF calculated for the LONEOS telescope. This PSF is appropriate for a scan-mode image taken from the edge of the CCD when observing near the zenith.

The general strategy used was to calculate a PSF appropriate to the wavelength and position on the CCD mosaic array, “read out” the model PSF accounting for those items listed above, and produce a realistic LONEOS PSF. Figure 2 shows an azimuthally asymmetric model PSF, and Fig. 3 shows how such PSFs are affected by their location within the focal plane; i.e., on the CCD mosaic. Figure 3 is based on ray-trace models of the LONEOS Schmidt telescope optical system. The asymmetric shape of the PSF is indeed a challenge to work with, but as will be seen, our method is rather general and does not depend on the shape of the PSF. The strength of the method is in its ability to use actual high-S/N PSFs from the camera itself as templates in generating our pixelized masks.

Once the model PSFs were produced, 2-D images of simulated data were generated that should closely match those produced by the LONEOS camera. The images were created by using our model PSFs as input to IRAF. By splitting each point source into 6 sub-objects and keeping the total brightness constant, we could offset the sub-objects slightly from their centers to form representations of the asymmetric LONEOS PSFs. The sub-objects were broadened into a rectangular shape to approximate the true PSF which will be smeared slightly in the scan (declination) direction (see bottom of Fig. 3). The per-pixel differences between the IRAF-generated LONEOS image PSFs and our initial single model PSF (Fig. 2) were small.

Our search and detection algorithms (described below) were then applied to these simulated images to discover how well we could find objects of known magnitude and position (see Sec. 5). In summary: At the zenith for a 68 sec integration, the limiting magnitude is $V \sim 19.8$ mag. We define “limiting magnitude” for a source to mean that magnitude at which an object will be detected in three overlapping scans at least 50% of the time. This same object will be detected in one scan $\sim 80\%$ of the time.

In order to set a cutoff S/N for initial detections, we

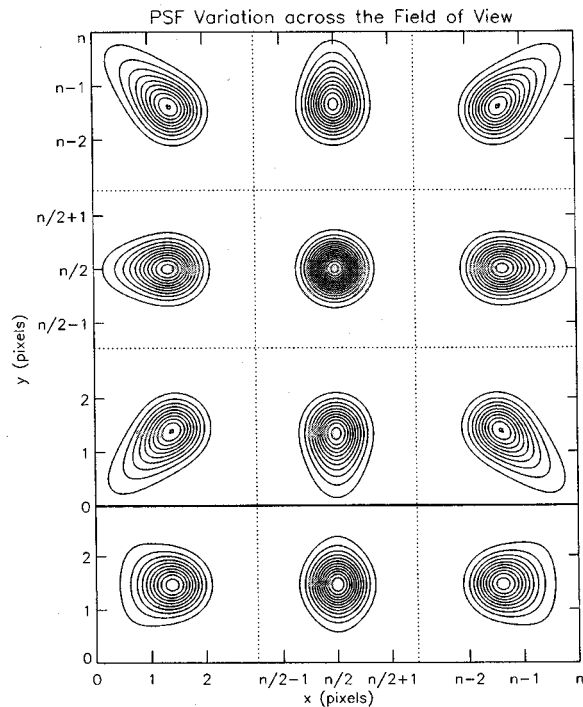


FIG. 3. Contour diagrams indicating schematically how the LONEOS PSF varies over the focal plane of the camera. The 9 PSFs in the top of the diagram indicate the way a star image would appear in a stare-mode frame where n is the total number of pixels in x or y (2048 in this case). As the point-source image approaches the edges of the CCD mosaic, chromatic aberration spreads the PSF. In scan mode, each point source will be transferred across the CCD from top to bottom. The bottom of this figure shows the resulting accumulated PSF as read from the camera. Each is the renormalized sum of the three PSFs above it.

looked at where our model PSFs could no longer be distinguished from noise in the majority of the cases. Figure 4 shows this graphically by plotting the total source counts against a normalized deviation from the known PSF, scaled such that zero deviation represents a perfect match between the input model and the output measured point source. We see from this figure that the onset of large deviations begin to occur for sources fainter than 20th magnitude, at which time the PSF tends towards being a single pixel event. Such single pixel events can *never* be separated from noise. The three most obvious conclusions from Fig. 4 are: (1) It is easy to define a cutoff value that will eliminate almost all single-pixel noise events; but (2) a few double pixel noise events will remain, and these are almost impossible to distinguish from faint point sources; and (3) it is impossible to distinguish single-pixel real events from single pixel noise events. The cutoff criterion we used was to examine any single pixel event 3.2σ or greater above the local noise floor and attempt to fit it with a pixel mask representative of a poorly sampled PSF. For double-pixel noise events to be eliminated, the cutoff threshold would have to be raised by ~ 0.5 mag. Using the three passes provided by the LONEOS scans, our PSF mask technique can be applied to each scan and we can accept or reject any source on the basis of the triple ensemble rather than on a single detection. Thus, at the very faint end

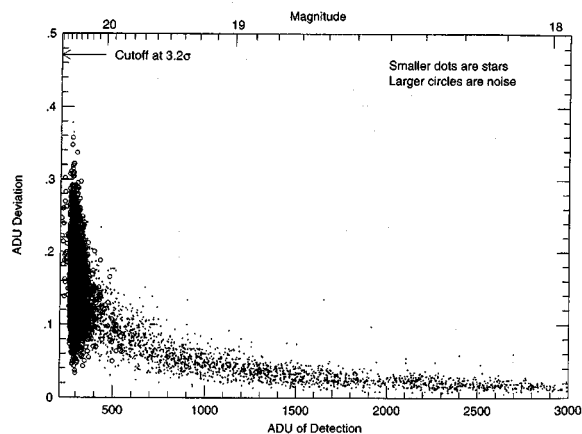


FIG. 4. Normalized deviation per pixel for detected sources from their input PSF. There are 4000 sources having a uniform magnitude distribution between 18 and 22. Deviations from the input PSF are plotted against the total (summed) counts for each detected source. The deviations were normalized by dividing by the total counts in each detection. The larger open circles (which accumulate into a dark region) are “detections” above the 3.2σ threshold that are really noise; small dots are the “real” (model input) point sources. Point sources fainter than ~ 20.5 mag were rarely detected, and the large area of accumulated sources (both noise and real) is the area comprising single-pixel events. The sharp cutoff is caused by very weak single-pixel events being “pushed” upward in total count by the PSF fit. Immediately to the right of this area are a small number of double-pixel noise events. The approximate V magnitude of a given source is also indicated.

our cutoff is determined by how many triples our computer can PSF fit in the available time.

Each candidate point source found by the initial 3.2σ threshold has its rough position and magnitude calculated at detection, using all adjacent pixels exceeding the cutoff value. The approximate center position is obtained by using simple (x,y) moment analysis and I is then estimated by using the sum of all adjacent pixels to assign an approximate brightness level. We then determine a good measure of the point-source center by finding the best match between the source and a sequence of generated pixelized PSF masks, each centered at 289 different sub-pixel positions² within the central pixel. Once the best-fit position is found, the pixelized mask is varied in brightness to produce a best-fit magnitude estimate. Both best-fit determinations are done by examining the absolute value of the sum of the differences in data-numbers between the template and the point source over all mask pixels.

Currently, the above work is based on model data as first light is not expected until summer 1996. However, using realistic model PSFs has allowed us to develop our techniques and to check the validity of our results. We have also been able to characterize the sensitivity of our methods to various camera and PSF parameters. The results shown in Fig. 3 make it clear that the appropriate PSF to use will depend on the location within the CCD mosaic. Once our initial PSF template is available (either from model data or from actual LONEOS data), it will form the basis for our

²The number 289 (17^2) was chosen because $1/17$ pixel is approaching the theoretical limit of spatial resolution and because an odd number of sub-pixels makes algorithm implementation easier.

generation of 289 marginally sampled or pixelized PSFs, each centered at $1/17$ pixel intervals, in both the x and y directions, all within a single pixel of the LONEOS CCD. The pixelized version of the PSF is calculated over a 5×5 -pixel area surrounding the source center³. When using actual LONEOS data, the method will produce exact PSFs.

Since the primary goal of the LONEOS project is to discover objects with non-sidereal motions, our CCD images are likely to contain some trailed sources. With a typical 68-second integration time, image trailing will become apparent when an object moves more than 1 deg/day. Since PSF masking, in the form presented here, is not an appropriate analysis technique for trailed objects, we do not consider them further in this paper. We also do not consider image asymmetries such as diffraction spikes.

In general, not all 25 pixels of the prototype PSFs need to be used. Each deviation calculation for a particular detection can be performed under a constant subset of the prototype called a fitting mask, the size and shape of which can be selected so the calculation is appropriate for the potential source based on an initial estimate of the S/N of total counts within a 5×5 box. For example, a very faint detection would use a small fitting mask, say 2×3 pixels, while a bright detection would use a larger fitting mask, possibly the full 5×5 size. For faint detections, most of the information will be contained in a two- or three-pixel area so a mask larger than 6 pixels would sample a region in which more than half the pixels contain only noise. This hybrid PSF fitting technique has the great advantage of always providing the optimum 2-D extraction aperture for a point source of any brightness, while making use of locally generated, well-sampled, high-S/N PSFs as the fitting models. This is a similar process to the growth curve analysis for faint stars discussed by Howell (1989). In the case of LONEOS, modeling indicates that use of a single 3×3 pixel mask is appropriate for all detections (see Table 2 and the next section). Use of a single small mask for all the LONEOS data also implies that only $9/25$ as many pixels are analyzed, thus saving CPU time.

We now discuss the PSF pixel-masking technique more formally. Let $P_{m,n}$ denote ideal pixelized point spread functions (pPSF) for the LONEOS system. The $P_{m,n}$ are calculated by placing the center of the ideal LONEOS PSF in equally spaced subpixels (m,n) on a central pixel and calculating the values of all pixels in the neighborhood. A 5×5 pixel area is sufficient to contain all significant pixelized values over the entire range of brightness imaged by the LONEOS camera. We adopt the custom of allowing m and n to have 17 different values: $-8 \leq m \leq 8$ and $-8 \leq n \leq 8$, where m,n are integers. In our notation, m indicates the RA direction and n indicates the DEC direction. The central position of the calculated PSF on the pixel is given by $\Delta x = m/17$ and $\Delta y = n/17$.

We denote an individual pixel value of a $P_{m,n}$, by $P_{m,n,x,y}$, where $-2 \leq x \leq 2$ and $-2 \leq y \leq 2$, with x,y being

³Although an unsaturated LONEOS point source image should seldom occupy more than 9 pixels, we allowed an extra pixel on each side of the mask for safety. This choice incurs no computational performance penalty.

TABLE 2. Results for LONEOS Gaussian profiles.^a

Magnitude	Sample Size	x-sigma (pixels)	y-sigma (pixels)	Magnitude Error
		x,y Centroiding; Pixel Summation		
17	4000	0.158	0.159	0.046
18	4000	0.151	0.150	0.102
19	4000	0.173	0.174	0.222
20	3002	0.278	0.279	0.335
PSF Pixel Masking Applied				
17	4000	0.030	0.030	0.044
18	4000	0.056	0.051	0.071
19	4000	0.129	0.130	0.148
20	3002	0.275	0.284	0.241

^aAt 20th magnitude, about one quarter of the sources were not detected as they were below our cutoff value.

integers. In this case, x represents the RA direction and y represents the DEC direction.

The $P_{m,n}$ are normalized so

$$\sum_{x=-2}^2 \sum_{y=-2}^2 P_{m,n,x,y} = 1$$

for all permitted m and n .

The software compares the 289 pPSFs to each potential detection and selects the pPSF that has the smallest deviation as the one that most accurately represents the image. To make such a comparison, the software must compute the approximate brightness of the object, D , and its approximate center (x_c, y_c) . These two quantities are provided by the initial search algorithm, which performs a simple moment analysis on all pixels above the cutoff value to find the center. It also sums the value of each pixel above the cutoff (and subtracts the average background) to find the approximate brightness. Then the deviation $E_{m,n}$ is calculated from

$$E_{m,n} = \sum_{x=-2}^2 \sum_{y=-2}^2 |I_{x+x_c, y+y_c} - DP_{m,n,x,y}|,$$

where $I_{x,y}$ is the DN value of the image pixel at (x,y) . This operation of simple sums is fast to compute.

Since, for our initial guess, we assume that the central pixel of the image contains the true subpixel center of the image, it is possible that we will miss the real center of an image that is located in an adjacent pixel. In actual tests of the software, we have found that by allowing the search to cross pixel boundaries, we can get very poor results. We attribute this to the fact that for very faint objects it is likely to be noise that is leading us across the pixel boundary. This type of pixel crossing produces large positional errors. Although our strategy of not allowing pixel boundary crossings may miss a few centers, overall it produces better results than a free-ranging search. We find in practice that we rarely miss the initial center by more than one pixel.

If an image was noiseless, we would expect the 2-D surface $E_{m,n}$ to contain points of a smooth function with a single minimum within the search area. Noise creates multiple minima within the search area, so it is to our advantage to examine each of the 289 $P_{m,n}$ to find the global minimum. Figure 5 provides a graphic representation of the space in which we are searching for a minimum. It shows $E_{m,n}$ over a

3×3 pixel region. This graph was generated from a typical "real" star, and provides clear evidence that the search space can have multiple, almost equal, local minima.

Our first guess of D , the total brightness in the image, is given by summing all adjacent pixels having DN above the cutoff. At the very least, our estimate of D omits contributions in the wings of the image (which may be in pixels below the cutoff), and it includes any noise contributions contained in the pixels above the cutoff. Small errors in the initial guess for D (a few 10s of percent) will not generally cause the incorrect pPSF to be chosen. Once a pPSF has been selected and fitted in x and y , the brightness of the potential detection can be determined more accurately. The brightness of the pPSF is varied until a minimum deviation between the selected pPSF and the actual image is found. This algorithm uses a Golden Section Search (Cheney & Kincaid 1980) to find the minimum deviation. The Golden Section Search finds a deviation minimum between two arbitrarily selected values of brightness. In this algorithm $D \pm 0.5D$, are used as the limits. These limits represent a compromise between wider search limits with a higher probability of finding the "correct" value and narrower limits with faster convergence. The algorithm assumes that there is exactly one minimum on the interval. It progressively narrows the search limits until a fixed small interval is obtained. At this point in the analysis, both the center of the image (x,y) and its brightness (I) are well determined by pPSF matching.

In the preceding discussion, we have again assumed that the deviation is calculated over all 25 pixels in the ideal pPSF. However, for the LONEOS camera there is almost never a situation where all 25 pixels are significant (i.e., source dominated) and using all 25 pixels only adds noise into the calculation. For the opposite situation where very bright objects contain pixels that are saturated, the saturated pixels and their contaminated neighbors are not included in the mask used in the analysis. Thus, both low S/N data and bright sources can be taken into account by the use of an appropriate pixel mask. Application of these pixel masks is straightforward. We start with a mask that is a 5×5 array that contains ones and zeros. If a pixel is to be analyzed the corresponding mask pixel contains a one; if a pixel is to be ignored, its corresponding mask pixel contains a zero. The

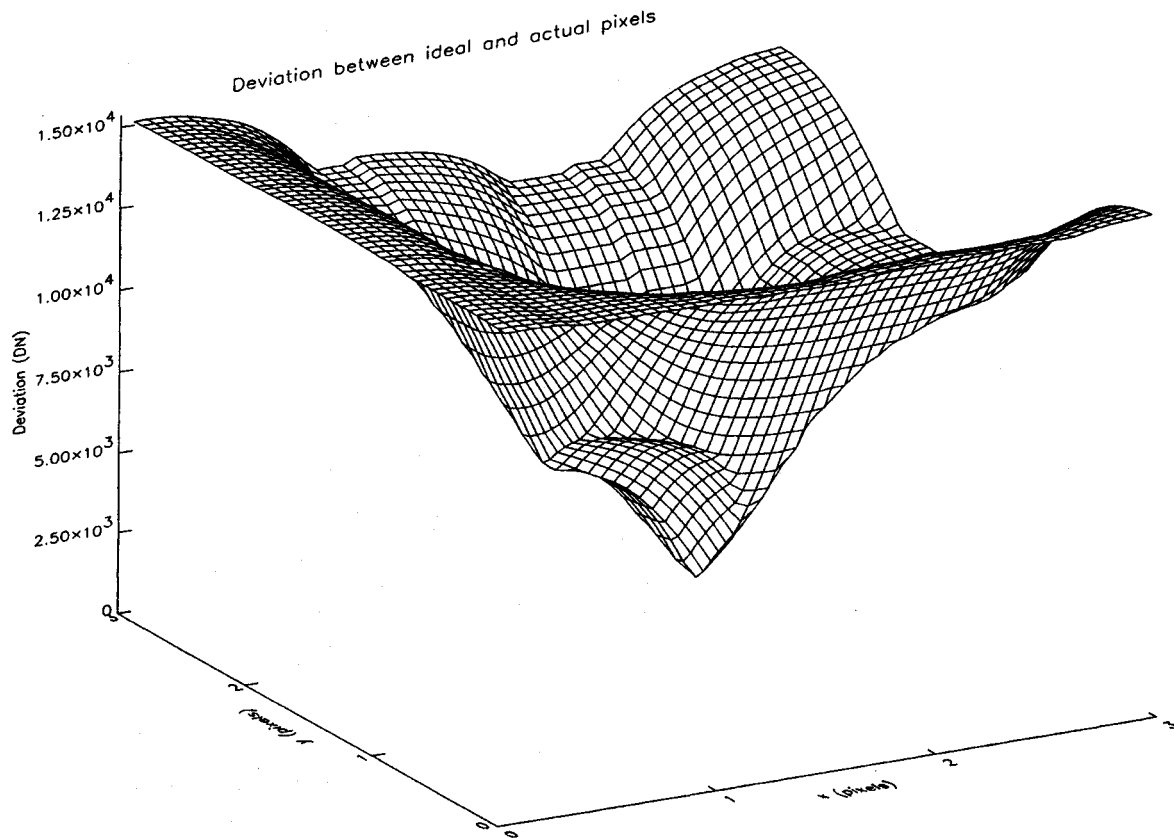


FIG. 5. Plot of the two-dimensional surface $E_{m,n}$ showing the deviation per pixel between an actual point source and the set of 289 possible pixelized PSF masks. The “lumps” in the surface are caused by the existence of more than one local minimum, and show that it is best to sample all subpixels to determine a best-fit minimum rather than seeking a single local minimum. The lumps are caused by noise in the PSF of the observed source.

mask, $M_{x,y}$, is then multiplied into the deviation calculation in the following way:

$$E_{m,n} = \sum_{x=-2}^2 \sum_{y=-2}^2 |I_{x+x_c, y+y_c} - DP_{m,n,x,y}| M_{x,y}.$$

For a CCD system having a larger dynamic range, that is, one in which different masks should be used for the entire range of point source brightness, the software will choose a mask based on the value of the initial guess of the total counts D . The size and shape of this mask will depend on the actual camera system used. If an image contains any saturated pixels, it can use a custom mask made of all 25 entries, but the saturated pixels and their (likely) contaminated neighbors will be zeroed.

5. RESULTS

To provide realistic noise modeling and image distortion, we used artificially generated point source frames as discussed above. We fitted a range of masks to each point source and examined the residuals for each. We first started with a LONEOS-sampled ($r=0.7$) pure Gaussian PSF and no mask fitting, and we determined the center by (x,y) cen-

troiding and the magnitude by a summation of the counts above the noise cutoff. Next, we used our PSF sampled variable pixel mask technique applied to the Gaussian profile to determine the center and the brightness. Finally, we applied PSF masking to the asymmetric best-guess LONEOS PSF (Fig. 2).

For the Gaussian profiles, we found that (x,y) centroiding worked fairly well when the sources were bright, but was poor for the faint (few-pixel) point sources. Application of the PSF mask technique greatly improved the center determinations and the magnitudes by decreasing the errors with respect to the generated data by up to factors of 5 in position and 2 in magnitude. These results are shown in Table 2 for a sample of 4000 point sources of magnitude 17 to 20. The errors in position are symmetric, as expected. The mask size used for the Gaussian profile tests here was 3×3 and these results are essentially the best one can expect for the faint end of the poorly sampled LONEOS sources and symmetric PSFs.

Using the expected *asymmetric* LONEOS PSF and PSF masking, we found the following. Even though there was a preference, as expected, for use of a larger mask for the brighter sources (the 5×5 mask giving slightly better results

TABLE 3. Results for different pixel mask sizes.

Magnitude	Sample Size	Mask Size	x -sigma	y -sigma	r -sigma
15.0	4096	5×5	0.084	0.216	0.232
		3×3	0.086	0.218	0.234
		2×3	0.364	0.321	0.388
		2×2	0.381	0.481	0.614
16.0	4096	5×5	0.031	0.091	0.097
		3×3	0.031	0.091	0.097
		2×3	0.105	0.101	0.146
		2×2	0.153	0.156	0.219
17.0	4096	5×5	0.037	0.080	0.088
		3×3	0.038	0.080	0.088
		2×3	0.082	0.083	0.117
		2×2	0.104	0.115	0.156
18.0	4096	5×5	0.069	0.068	0.097
		3×3	0.070	0.068	0.098
		2×3	0.129	0.074	0.149
		2×2	0.143	0.125	0.190
19.0	4096	5×5	0.134	0.121	0.181
		3×3	0.134	0.121	0.181
		2×3	0.189	0.122	0.225
		2×2	0.198	0.174	0.264
19.5	4039	5×5	0.208	0.195	0.285
		3×3	0.207	0.196	0.285
		2×3	0.256	0.198	0.323
		2×2	0.263	0.242	0.358
19.7	3857	5×5	0.246	0.226	0.335
		3×3	0.244	0.225	0.332
		2×3	0.279	0.228	0.360
		2×2	0.287	0.261	0.388
19.9	3393	5×5	0.271	0.253	0.371
		3×3	0.270	0.249	0.368
		2×3	0.292	0.249	0.384
		2×2	0.299	0.277	0.408
20.1	2729	5×5	0.292	0.280	0.404
		3×3	0.289	0.277	0.401
		2×3	0.304	0.280	0.413
		2×2	0.311	0.298	0.431
20.3	1935	5×5	0.313	0.309	0.440
		3×3	0.313	0.310	0.440
		2×3	0.321	0.305	0.443
		2×2	0.327	0.313	0.453

down to near 18th magnitude and being clearly superior for the brighter sources; $V > 15$ mag), we found that in the case of the LONEOS data, use of a single mask of size 3×3 , provides good results over the entire range of detection. Table 3 shows the results of this test, based on using 4096 generated point sources. We see that the error is always greater in the y (declination) direction due to image smear, even for PSFs located near the center of the focal plane. Using the results in Fig. 4 and Table 3 allows one to set software criteria which, during reduction, can choose the PSF pixel mask to use for optimum S/N results for each point source.

TABLE 4. Calculated 1σ errors for LONEOS PSFs.

Magnitude	1σ Magnitude Error ^a	1σ Error ^b (pixels)	1σ Error ^b (arcsec)
15	0.006	0.234	0.655
16	0.013	0.097	0.272
17	0.032	0.088	0.246
18	0.078	0.098	0.274
19	0.195	0.181	0.507
20	0.489	0.384	1.074
20.5	0.774	0.440	1.232

^aCalculated using the results of this paper and Eq. (6) in Howell 1993.

^bPoor results at 15th magnitude are due to some saturated pixels.

We can use a single 3×3 pixel mask in this case due to the limited dynamic range of the MPP run detectors, which have full well depths of $\sim 100,000$ electrons. One also sees that as the point sources became fainter, some number of them ($\sim 2\%$ at 19.5 mag to $\sim 20\%$ at 20 mag) were not detected on the simulated frames by our initial search at its predefined cutoff level. We find again that the limiting magnitude, with fairly complete detections, is near $V = 19.8$ mag. Undersampled images have a slight advantage with our technique, in that low-S/N objects are easier to detect as most of their light is contained within a few pixels. If the sampling parameter were worse, that is, if the real PSF were much smaller than the pixel size, then an accurate position for the source center becomes difficult to know and intrapixel non-uniformities (Jordan *et al.* 1994) also make the brightness uncertain.

Using our preferred mask size of 3×3 pixels, we can estimate the performance of our methods, as applied to the LONEOS camera, in terms of astrometric and photometric precision. Based on numerous runs with model data as well as application of the rigorous error analysis (Merline & Howell 1995), we can provide error estimates for the range of LONEOS magnitudes. These are given in Table 4. While we believe that a realistic limiting magnitude will be near $V = 19.5$ mag, we have listed the determined errors down to $V = 20.5$ mag. As can be seen from Table 4, the errors are exceptionally small given the parameter space of pixel size and total counts we have to work with, and are not too much worse than those for a symmetric Gaussian PSF (Table 2). The numbers in Table 4 are a reflection of the robustness of our technique.

6. CONCLUSIONS

Poorly sampled data provide a bountiful regime in which astronomers can work. However, the literature gives few suggestions on techniques for making optimal use of these data. We have shown that traditional ways of analyzing data are not adequate for poorly sampled data and have proposed a technique that greatly improves on traditional methods. The method uses pixel masks for the PSF fitting. PSF masking is implemented by creating a series of masks formed by pixelizing an ideal PSF with various pixel centers. Each of these masks is then compared to a point source of interest, and the best-fit mask taken as providing an accurate center. The brightness of the now centered mask is then varied, allowing a good determination of the source intensity.

Critical to fitting pixel masks is determining the real PSF. We have indicated that the PSF is not constant in the LONEOS instrument, but varies as a function of its position on the CCD perpendicular to the scan direction. When scanning, the PSF essentially becomes the sum of all PSFs in a vertical column on the CCD. Consequently, the PSFs vary only as a function of the distance across the CCD perpendicular to the scan direction. Application to real images will consist of construction of an approximate PSF by summing a large number (several hundred) of bright, unsaturated star images. Since we know the PSF varies across the LONEOS CCD mosaic, we will build several approximate PSFs, one for each of several pre-defined regions of the CCD. Finally, each of these approximate PSFs is pixelized into masks used in the PSF masking technique described above.

In CCD imaging systems that have a broad dynamic range, the number of pixels within the mask over which the PSF is sampled, has a significant bearing on the result and should be changed to suit the point source of interest. Faint objects that cover few pixels should use a small mask to exclude pixels that would otherwise add noise to the analysis. Bright images should use a larger mask so all the signal-containing pixels are included. If a star image is saturated, a mask can be used to remove those pixels spoiled by saturation. All point sources are thus optimized for maximum S/N.

Applying this technique to the LONEOS system, we have tested the algorithms on simulated data with good results.

The 1σ error for positions and magnitudes are significantly better than the error using moment analysis and pixel summation (DN level addition) alone. The faint limit for point source work is also greatly extended. Attempting to fit Gaussian PSFs to the simulated data produced unusable results. We have also found that a variable mask size does not help the LONEOS analysis because of the somewhat limited dynamic range of the LONEOS camera. The overall astrometric and photometric errors predicted for LONEOS point sources are far better than would be possible using traditional techniques.

We wish to thank David Dodgen, formerly of Dodgen Optical Co. (Flagstaff, Arizona) for his contributions on the optical design and ray tracing of the LONEOS camera, Christopher Stubbs and Alan Diercks (University of Washington) for their work on the LONEOS camera and for providing us with numerous specifications related to its operation and noise properties, and to David Monet (US Naval Observatory Flagstaff Station) for providing software support. We also wish to thank G. Jacoby, L. Davis, and T. Abbott for their comments on CCD photometric techniques. Finally, the authors would like to acknowledge the time and effort expended reviewing this paper by the referee. This research was supported, in part, by NASA grant NAGW-3397.

REFERENCES

- Abbott, T. M. C. 1993, Ph. D. thesis, University of Texas
- Adams, M., Christian, C., Mould, J., Stryker, L., & Tody, D. 1980, *Stellar Magnitudes from Digital Pictures* (Kitt Peak National Observatory, Tucson, Arizona)
- Bowell, E., & Muinonen, K., 1994, in *Hazards Due to Comets and Asteroids*, edited by T. Gehrels (University of Arizona Press, Tucson)
- Buonanno, R., & Iannicola, G. 1989, *PASP*, 101, 294
- Cheney, W., & Kincaid, D. 1980, *Numerical Methods and Computing* (Brooks/Cole Publishing Co., Belmont, MA), Chap. 10
- Diercks, A., *et al.* 1995, *Proc. SPIE*, Vol. 2416
- Goad, L. 1986, *Proc. SPIE* 1, 627, Part 2, 688
- Holtzman, J. A. 1990, *PASP*, 102, 806
- Holtzman, J. A., *et al.* 1995, *PASP*, 107, 156
- Howell, S. B. 1989, *PASP*, 101, 616
- Howell, S. B., & Merline, W. J. 1991, *Galileo Project SSI Calibration Report*, JPL Galileo Memo, Oct 25
- Howell, S. B. 1993, in *Stellar Photometry — Current Techniques and Future Developments*, IAU Colloquium No. 136, edited by C. J. Butler and I. Elliott (Cambridge University Press, Cambridge), p. 318
- Howell, S. B., 1995, in *New Developments in Array Technology and Applications*, IAU Symposium No. 167, edited by A. G. Davis Philip, K. A. Janes, and A. R. Uggren (Kluwer, Dordrecht), p. 167
- Jorden, P. R., Deltorn, J-M., & Oates, A. P. 1994, *Proceedings of Instrumentation in Astronomy VIII*, SPIE Vol. 2198 (SPIE, Bellingham), p. 57
- Massey, P., Gronwall, C., & Pilachowski, C. 1990, *PASP*, 102, 1046
- Merline, W. J., & Howell, S. B. 1995, *Exp. Astron.*, 6, 163
- Shoemaker, E. M. 1995, *Report of Near-Earth Objects Survey Working Group* NASA
- Stetson, P. 1987, *PASP*, 99, 191
- Tüg, H., White, N. M., & Lockwood, G. W. 1977, *A&A*, 61, 679